

## ACCELERATING MULTIGRID OPTIMIZATION VIA SESOP\*

TAO HONG, IRAD YAVNEH AND MICHAEL ZIBULEVSKY

**Abstract.** A merger of two optimization frameworks is introduced: SEquential Subspace OPtimization (SESOP) with the MultiGrid (MG) optimization. At each iteration of the algorithm, search directions implied by the coarse-grid correction (CGC) process of MG are added to the low dimensional search-spaces of SESOP, which include the (preconditioned) gradient and search directions involving the previous iterates (so-called history). The resulting accelerated technique is called SESOP-MG. The asymptotic convergence factor of the two-level version of SESOP-MG (dubbed SESOP-TG) is studied via Fourier mode analysis for linear problems, i.e., optimization of quadratic functionals. Numerical tests on linear and nonlinear problems demonstrate the effectiveness of the approach.

**Key words.** SESOP, acceleration, multigrid, history, linear and nonlinear large-scale problems

**AMS subject classifications.** 65N55, 65N22, 65H10

**1. Introduction.** MultiGrid (MG) methods are widely considered as a highly efficient approach for solving elliptic partial differential equations (PDEs) and systems, as well as other problems which can be effectively represented on a hierarchy of grids or levels. However, it is not always easy to design efficient MG methods for difficult problems, and therefore MG methods are often used in combination with acceleration techniques (e.g., [16]). Basically, there are two challenges in developing MG algorithms: choosing a cheap and effective smoother, often called Relaxation, and designing a useful coarse-grid problem, whose solution yields a good coarse-grid correction (CGC). Imperfect choices of the latter often results in a deterioration of the convergence factors when many levels are used in the MG hierarchy, and the MG algorithm is not robust.

In this manuscript we study MG in an optimization framework and seek robust solution methods by merging this approach with so-called SEquential Subspace OPtimization (SESOP) [26] to obtain a robust solver. SESOP belongs to a general framework for addressing large-scale optimization problems, as described in the next section. The combined framework is called SESOP-MG, and its two-level version SESOP-TG. We analyze the convergence factor of a fixed stepsize version of SESOP-TG for quadratic optimization problems, and thus quantify the expected acceleration due to SESOP by means of the so-called h-ellipticity measure [3, 20]. Numerical experiments demonstrate the relevance of the theoretical analysis and the effectiveness of the proposed scheme for linear and nonlinear problems.

The paper is organized as follows. The standard MG and SESOP algorithms are briefly described in Section 2. We then introduce the SESOP-TG / SESOP-MG algorithm in Section 3 and analyze the fixed stepsize SESOP-TG method for quadratic problems. Numerical results in Section 4 demonstrate the effectiveness of SESOP-MG for solving linear and nonlinear problems. Conclusions are drawn in Section 5.

We adopt the following notation throughout this paper. In the two-grid case, we use superscripts  $h$  and  $H$  to denote the fine and coarse grid. We assume  $H = 2h$ , although more aggressive coarsening may also be considered. Specifically,  $\mathcal{F}^h(\mathbf{x}^h)$  and  $\mathcal{F}^H(\mathbf{x}^H)$  denote the fine and coarse functions, respectively. The notation  $\nabla \mathcal{F}^h(\mathbf{x}^h)$

---

\*Submitted to the editors DATE.

**Funding:** This work was funded by \*\*\*\*

and  $\nabla \mathcal{F}^H(\mathbf{x}^H)$  is used for the gradients of  $\mathcal{F}^h(\mathbf{x}^h)$  and  $\mathcal{F}^H(\mathbf{x}^H)$ , respectively. For MG, we use  $\mathcal{F}_{l,k}(\mathbf{x}_{l,k})$  to denote the  $l$ -level function at the  $k$ th iteration where  $l = 1$  denotes the finest level and  $l = L$  the coarsest one, assuming a total of  $L$  levels. We use boldface font to denote vectors and matrices, and  $^T$  denotes the transpose operator.

**2. Preliminaries.** In this section we briefly describe MG and SESOP—the building-blocks of SESOP-MG, which are merged in the next section.

**2.1. MultiGrid (MG).** MG methods are considered to be amongst of the most efficient numerical approaches for solving large-scale systems of equations (linear and non-linear) arising from the discretization of elliptic partial differential equations (PDEs) [2, 5, 18, 25]. In [14], Nash formulated the MG method in an optimization framework called MG/OPT which is closely related to the well-known full approximation storage (FAS) scheme [2]. Following this, Lewis and Nash utilized this framework to solve the optimization of systems governed by differential equations [12]. Following the same framework, Wen and Goldfarb proposed a line search MG method to solve the unconstrained convex and nonconvex problems [21]. Toint et al. merged the MG methods with the trust region methods, applying the MG methods to solving the series of linear subproblems arising in each step of trust region methods, to handle the nonlinear convex or nonconvex problems even with bound constraints [9, 10, 19, 8]. Moreover, Borzi and Schulz [1] reviewed several works on applying MG methods for optimization problems such as shape design, parameter optimization, and optimal control problems governed by PDEs. These types of methods can be viewed as an acceleration of simple and inexpensive traditional iterative methods based on local relaxation, e.g., Jacobi or Gauss-Seidel. Such methods are typically very efficient at reducing errors that are oscillatory with respect to the computational grid, but inefficient for errors that are relatively “smooth”, that is, undergo little change over the span of a few mesh intervals. The main idea in MG methods is to project the equation for the error remaining after applying a few iterations of local relaxation onto a coarser grid. This yields two advantages. First, the resulting coarse-grid system is smaller, hence cheaper to solve. Second, part of the slowly converging smooth error on a finer grid becomes relatively more oscillatory on the coarser grid, and therefore can be treated more efficiently by a local relaxation method. Thus, the coarse-grid problem is treated recursively, by applying relaxation and projecting to a still coarser grid resulting in a multilevel hierarchy. Once the coarse-grid problem is solved approximately, its solution is prolonged and added to the fine-grid approximation—this is called coarse-grid correction.

In preparation towards merging MG with SESOP, we cast our problem in variational form as a nested hierarchy of optimization problems (see, e.g., [10, 14]). We adopt the common MG notation, where it is assumed that the function we wish to minimize is defined on a grid with nominal mesh-size  $h$  and is denoted  $\mathcal{F}^h$ . For simplicity, we consider the two-level (or two-grid) framework, with the coarse-grid mesh-size denoted by  $H$ , and discuss the extension to multilevels later.

Consider the following unconstrained problem defined on the fine-grid:

$$(2.1) \quad \mathbf{x}_*^h = \underset{\mathbf{x}^h \in \mathbb{R}^N}{\operatorname{argmin}} \mathcal{F}^h(\mathbf{x}^h),$$

where  $\mathcal{F}^h(\mathbf{x}^h) : \mathbb{R}^N \rightarrow \mathbb{R}$  is a differentiable function and the solution set of (2.1) is not empty. Let  $\mathbf{x}_k^h$  denote our approximation to the fine-grid solution  $\mathbf{x}_*^h$  after the  $k$ th iteration. Assume that we have defined a *restriction* operator  $\mathbf{I}_h^H : \mathbb{R}^N \rightarrow \mathbb{R}^{N_c}$ ,

and a *prolongation* operator  $\mathbf{I}_H^h : \mathfrak{R}^{N_c} \rightarrow \mathfrak{R}^N$ , where  $N_c$  is the size of the coarse grid. Furthermore, let  $\mathbf{x}_k^H$  denote a coarse-grid approximation to  $\mathbf{x}_k^h$  (for example, we may use  $\mathbf{x}_k^H = \mathbf{I}_H^h \mathbf{x}_k^h$ , but other choices may be used as well). The coarse-grid problem is then defined as follows:

$$(2.2) \quad \mathbf{x}_*^H = \operatorname{argmin}_{\mathbf{x}^H \in \mathfrak{R}^{N_c}} \mathcal{F}^H(\mathbf{x}^H) - \mathbf{v}_k^T \mathbf{x}^H,$$

where  $\mathcal{F}^H$  is a coarse approximation to  $\mathcal{F}^h$ , and  $\mathbf{v}_k = \nabla \mathcal{F}^H(\mathbf{x}_k^H) - \mathbf{I}_H^H \nabla \mathcal{F}^h(\mathbf{x}_k^h)$ . The correction term  $\mathbf{v}_k$  is used to enforce the same first-order optimality condition [14] on the fine and coarse levels. After solving (2.2) (by some method), the CGC direction is given by

$$(2.3) \quad \mathbf{d}_k^h = \mathbf{I}_H^h \mathbf{d}_k^H = \mathbf{I}_H^h (\mathbf{x}_*^H - \mathbf{x}_k^H).$$

Finally, the CGC is prolonged and added to the current fine-grid approximation:

$$(2.4) \quad \mathbf{x}_{k+1}^h = \mathbf{x}_k^h + \mathbf{d}_k^h.$$

This may be followed by additional relaxation steps.

**2.2. SEquential Subspace OPTimization (SESOP).** We are concerned with the solution of smooth large-scale unconstrained problems

$$(2.5) \quad \min_{\mathbf{x} \in \mathfrak{R}^N} \mathcal{F}(\mathbf{x}).$$

The SESOP approach [13, 6, 27, 26] is an established framework for solving (2.5) by sequential optimization over affine subspaces  $\mathcal{M}_k$ , spanned by the current descent direction (typically preconditioned gradient) and  $\Pi$  previous propagation directions of the method. If  $\mathcal{F}(\mathbf{x})$  is convex, SESOP yields the optimal worst-case convergence factor of  $O(\frac{1}{k^2})$  [13], while achieving efficiency of the quadratic Conjugate-Gradient (CG) method when the problem is close to quadratic or in the vicinity of the solution.

The affine subspace at the iteration  $k$  is defined by

$$\mathcal{M}_k = \{\mathbf{x}_k + \mathbf{P}_k \boldsymbol{\alpha} : \boldsymbol{\alpha} \in \mathfrak{R}^{\Pi+1}\},$$

where  $\mathbf{x}_k$  is the  $k$ th iterate, the matrix  $\mathbf{P}_k$  contains the spanning directions in its columns, the preconditioned gradient  $\boldsymbol{\Phi} \nabla f(\mathbf{x}_k)$  and  $\Pi$  last steps  $\boldsymbol{\delta}_i = \mathbf{x}_i - \mathbf{x}_{i-1}$ ,

$$(2.6) \quad \mathbf{P}_k = [\boldsymbol{\Phi} \nabla \mathcal{F}(\mathbf{x}_k), \boldsymbol{\delta}_k, \boldsymbol{\delta}_{k-1}, \dots, \boldsymbol{\delta}_{k-\Pi+1}], \quad \Pi \geq 0.$$

The new iterate  $\mathbf{x}_{k+1}$  is obtained via optimization of  $\mathcal{F}(\cdot)$  over the current subspace  $\mathcal{M}_k$ ,

$$(2.7) \quad \begin{aligned} \tilde{\boldsymbol{\alpha}} &= \operatorname{argmin}_{\boldsymbol{\alpha} \in \mathfrak{R}^{\Pi+1}} \mathcal{F}(\mathbf{x}_k + \mathbf{P}_k \boldsymbol{\alpha}), \\ \mathbf{x}_{k+1} &= \mathbf{x}_k + \mathbf{P}_k \tilde{\boldsymbol{\alpha}}. \end{aligned}$$

By keeping the dimension of  $\boldsymbol{\alpha}$  low, (2.7) can be solved efficiently with a Newton-type method. SESOP is relatively efficient if the following two conditions are satisfied:

- The objective function can be represented as  $\Omega(\mathbf{A}\mathbf{x})$ .
- Evaluation of  $\Omega(\cdot)$  is cheap, but calculating  $\mathbf{A}\mathbf{x}$  is expensive.

In this case, storing  $\mathbf{A}\mathbf{P}_k$  and  $\mathbf{A}\mathbf{x}_k$ , we can avoid re-computation of  $\mathbf{A}\mathbf{x}_k$  during the subspace minimization. A typical class of problems of this type is the well-known  $\ell_1 - \ell_2$  optimization [27].

SESOP can yield faster convergence if more efficient descent directions are added to the subspace  $\mathcal{M}_k$ . This may include a cumulative or parallel coordinate descent step, a separable surrogate function or expectation-maximization step, Newton-type steps and other methods [6, 27, 26]. In this work we suggest adding the CGC direction provided by the MG framework.

**3. Merging SESOP with Multigrid.** As noted above, the main idea we are pursuing in this manuscript is merging the SESOP optimization framework with MG by enriching the SESOP subspace  $\mathbf{P}_k$  with one or more directions implied by the CGC. We expect that robust and efficient algorithms for large-scale optimization problems may be obtained through such a merger in cases where a multi-scale hierarchy can be usefully defined. Numerical experiments presented in Section 4 for linear and nonlinear problems demonstrate the potential advantage of this approach. Moreover, the convergence factor analysis of SESOP-TG for the quadratic case in Subsection 3.1 also indicates the potential merits of merging SESOP with MG.

We begin this section by introducing a two-grid version of our scheme first, SESOP-TG, and later extend it to a multilevel version, SESOP-MG. At its basic form, the idea is to add the coarse correction  $\mathbf{d}_k^h$  of (2.3) into the affine subspace  $\mathbf{P}_k$ , obtaining the augmented subspace  $\tilde{\mathbf{P}}_k = [\mathbf{d}_k^h \quad \mathbf{P}_k]$ . We then replace  $\mathbf{P}_k$  by  $\tilde{\mathbf{P}}_k$  in (2.7) and compute the locally optimal  $\boldsymbol{\alpha}$  to obtain the next iterate,  $\mathbf{x}_{k+1}$ . Our intention is to combine the efficiency of MG that results from fast reduction of large-scale error by the CGC, with the robustness of SESOP that results from the local optimization over the subspace. That is, even in difficult cases where the CGC is poor, the algorithm should still converge at least as fast as the standard SESOP, because an inefficient direction simply results in small (or conceivably even negative) weighting. SESOP-TG is presented in Algorithm 3.1. Note that we add the option of two additional steps to the usual SESOP algorithm, the pre- and post-relaxation steps 2 and 7 in Algorithm 3.1, commonly applied in MG algorithms. This allows us to advance the solution with low computational expense whenever the coarse-grid direction is highly inefficient.

**3.1. Convergence factor analysis for fixed stepsize SESOP-TG for quadratic problems.** To gain insight, we analyze our proposed algorithm for quadratic optimization problems that are equivalent to the solution of linear systems. We first derive a rather general formulation for the case of SESOP-TG with a single history ( $\Pi = 1$ ). Then, we explore further under certain simplifying assumptions. In this analysis we assume no pre- or postrelaxation steps.

Consider the linear system

$$(3.1) \quad \mathbf{A}\mathbf{x} = \mathbf{f},$$

where  $\mathbf{A} \in \mathbb{R}^{N \times N}$  is a symmetric positive-definite (SPD) matrix and we omit  $h$  superscripts for notational simplicity. Evidently, solving (3.1) is equivalent to the following quadratic minimization problem:

$$(3.2) \quad \mathbf{x}^* = \underset{\mathbf{x} \in \mathbb{R}^N}{\operatorname{argmin}} \mathcal{F}(\mathbf{x}) \triangleq \frac{1}{2} \mathbf{x}^\top \mathbf{A} \mathbf{x} - \mathbf{f}^\top \mathbf{x}.$$

Given iterates  $\mathbf{x}_{k-1}$  and  $\mathbf{x}_{k-2}$ , the next iterate produced by SESOP-TG with a single

**Algorithm 3.1** SESOP-TG

**Initialization:** Initial value  $\mathbf{x}_1^h$ , total number of iterations  $Iter_{max}$ , size of subspace  $\Pi \geq 0$ , the preconditioner  $\Phi$  and  $v_1, v_2$  – the number of pre- and postrelaxation steps.

**Output:** Solution:  $\mathbf{x}_*^h$

- 1: **for**  $k = 1 : Iter_{max}$  **do**
- 2:  $\mathbf{x}_k^h \leftarrow Relaxation(\mathbf{x}_k^h, v_1)$
- 3: Calculate the gradient:  $\nabla \mathcal{F}^h(\mathbf{x}_k^h)$  and formulate the subspace  $\mathbf{P}_k \leftarrow [\Phi \nabla \mathcal{F}^h(\mathbf{x}_k^h) \quad \mathbf{x}_k^h - \mathbf{x}_{k-1}^h \quad \cdots \quad \mathbf{x}_{k-\Pi+1}^h - \mathbf{x}_{k-\Pi}^h]$
- 4: Solve the coarse problem (2.2), obtaining  $\mathbf{x}_*^H$ .
- 5: Compute the coarse correction  $\mathbf{d}_k^h = \mathbf{I}_H^h (\mathbf{x}_*^H - \mathbf{I}_h^H \mathbf{x}_k^h)$  and set the subspace  $\bar{\mathbf{P}}_k \leftarrow [\mathbf{d}_k^h \quad \mathbf{P}_k]$ .
- 6: Solve approximately (2.7) on  $\bar{\mathbf{P}}_k$  and update  $\mathbf{x}_{k+1}^h \leftarrow \mathbf{x}_k^h + \bar{\mathbf{P}}_k \boldsymbol{\alpha}_k$ .
- 7:  $\mathbf{x}_{k+1}^h \leftarrow Relaxation(\mathbf{x}_{k+1}^h, v_2)$
- 8: **end for**
- 9:  $\mathbf{x}_*^h \leftarrow \mathbf{x}_{Iter_{max}+1}^h$
- 10: **return**

history is given by

$$(3.3) \quad \mathbf{x}_k = \mathbf{x}_{k-1} + c_1(\mathbf{x}_{k-1} - \mathbf{x}_{k-2}) + c_2 \Phi(\mathbf{f} - \mathbf{A}\mathbf{x}_{k-1}) + c_3 \mathbf{I}_H^h \mathbf{A}_H^{-1} \mathbf{I}_h^H (\mathbf{f} - \mathbf{A}\mathbf{x}_{k-1}),$$

where  $c_1, c_2, c_3$  are the locally optimal weights associated with the three directions comprising  $\mathbf{P}_k$ :  $c_1$  multiplies the so-called history, that is, the difference between the last two iterates;  $c_2$  multiplies the preconditioned gradient;  $c_3$  multiplies the CGC direction  $\mathbf{d}_{k-1}^h$ . Here,  $\mathbf{A}_H$  represents the coarse-grid matrix approximating  $\mathbf{A}$ , which is most commonly defined by the Galerkin formula,  $\mathbf{A}_H = \mathbf{I}_h^H \mathbf{A} \mathbf{I}_h^h$ , or simply by rediscrretization on the coarse-grid in the case where  $\mathbf{A}$  is the discretization of an elliptic partial differential equation on the fine-grid. Subtracting  $\mathbf{x}^*$  from both sides of (3.3), and denoting the error by  $\mathbf{e}_k = \mathbf{x}^* - \mathbf{x}_k$ , we get

$$(3.4) \quad \mathbf{e}_k = \mathbf{e}_{k-1} + c_1(\mathbf{e}_{k-1} - \mathbf{e}_{k-2}) - c_2 \Phi \mathbf{A} \mathbf{e}_{k-1} - c_3 \mathbf{I}_H^h \mathbf{A}_H^{-1} \mathbf{I}_h^H \mathbf{A} \mathbf{e}_{k-1}.$$

Rearranging (3.4) yields

$$(3.5) \quad \mathbf{e}_k = \mathbf{\Gamma} \mathbf{e}_{k-1} - c_1 \mathbf{e}_{k-2},$$

where

$$(3.6) \quad \mathbf{\Gamma} = (1 + c_1) \mathbf{I} - (c_2 \Phi + c_3 \mathbf{I}_H^h \mathbf{A}_H^{-1} \mathbf{I}_h^H) \mathbf{A},$$

and  $\mathbf{I}$  denotes the identity matrix. Define the vector  $\mathbf{E}_k = \begin{bmatrix} \mathbf{e}_k \\ \mathbf{e}_{k-1} \end{bmatrix}$ . Then, (3.5) implies the following relation:

$$(3.7) \quad \mathbf{E}_k = \mathbf{\Upsilon} \mathbf{E}_{k-1}, \quad \mathbf{\Upsilon} \triangleq \begin{bmatrix} \mathbf{\Gamma} & -c_1 \mathbf{I} \\ \mathbf{I} & \mathbf{0} \end{bmatrix}.$$

To analyze the convergence factor of SESOP-TG, we will continue under the assumption that the coefficients  $c_j$ ,  $j = 1, \dots, 3$  do not change from iteration to iteration, and we will search for the optimal fixed coefficients. In practice, the coefficients

do vary but we will verify numerically that the analysis is nonetheless very relevant inasmuch as the SESOP-TG convergence history curve oscillates around the optimal fixed- $c_j$  curve, so there is a near-match in an average sense. For fixed  $c_j$ , the asymptotic convergence factor of the SESOP-TG iteration is determined by the spectral radius of  $\Upsilon$ . Let  $r$  denote an eigenvalue of  $\Upsilon$  with eigenvector  $\mathbf{v} = [\mathbf{v}_1, \mathbf{v}_2]^T$ :

$$\begin{bmatrix} \mathbf{\Gamma} & -c_1 \mathbf{I} \\ \mathbf{I} & \mathbf{0} \end{bmatrix} \begin{bmatrix} \mathbf{v}_1 \\ \mathbf{v}_2 \end{bmatrix} = r \begin{bmatrix} \mathbf{v}_1 \\ \mathbf{v}_2 \end{bmatrix}.$$

Hence,  $\mathbf{v}_1 = r\mathbf{v}_2$  and  $\mathbf{\Gamma}\mathbf{v}_1 - c_1\mathbf{v}_2 = r\mathbf{v}_1$ . This yields

$$\mathbf{\Gamma}\mathbf{v}_1 = \left(r + \frac{c_1}{r}\right) \mathbf{v}_1.$$

Thus,  $\mathbf{v}_1$  is an eigenvector of  $\mathbf{\Gamma}$  with eigenvalue  $b = r + \frac{c_1}{r}$ . This leads to the following quadratic equation:

$$r^2 - br + c_1 = 0,$$

with solutions

$$r_{1,2} = \frac{1}{2} \left( b \pm \sqrt{b^2 - 4c_1} \right).$$

The asymptotic convergence factor is given by the spectral radius of  $\Upsilon$ ,

$$(3.8) \quad \rho(\Upsilon) = \max_b \left| \frac{1}{2} \left( b \pm \sqrt{b^2 - 4c_1} \right) \right|,$$

where  $b$  runs over the eigenvalues of  $\mathbf{\Gamma}$ . For the remainder of our analysis we focus on the case where the eigenvalues  $b$  of  $\mathbf{\Gamma}$  are all real.

**3.1.1. The case of real  $b$ .** In many practical cases, the eigenvalues of  $\mathbf{\Gamma}$  are all real, which simplifies the analysis and yields insight. We focus next on a common situation where this is indeed the case.

LEMMA 3.1. *Assume:*

1. *The prolongation has full column-rank and the restriction is the transpose of the prolongation:  $\mathbf{I}_h^H = (\mathbf{I}_H^h)^T$  (optionally up to a positive multiplicative constant).*
2. *The coarse-grid operator  $\mathbf{A}_H$  is SPD.*
3. *The preconditioner  $\mathbf{\Phi}$  is SPD.*

*Then the eigenvalues of  $\mathbf{\Gamma} = (1 + c_1)\mathbf{I} - (c_2\mathbf{\Phi} + c_3\mathbf{I}_H^h\mathbf{A}_H^{-1}\mathbf{I}_h^H)\mathbf{A}$  are all real.*

*Proof.* Because  $\mathbf{A}$  is SPD, there exists a SPD matrix  $\mathbf{S} = \sqrt{\mathbf{A}}$  such that  $\mathbf{S}^2 = \mathbf{A}$ . The matrix

$$\mathbf{S}\mathbf{\Gamma}\mathbf{S}^{-1} = (1 + c_1)\mathbf{I} - \mathbf{S}(c_2\mathbf{\Phi} + c_3\mathbf{I}_H^h\mathbf{A}_H^{-1}\mathbf{I}_h^H)\mathbf{S}$$

is similar to  $\mathbf{\Gamma}$  so they have the same eigenvalues. Moreover,  $\mathbf{S}\mathbf{\Gamma}\mathbf{S}^{-1}$  is evidently symmetric, so its eigenvalues are all real.  $\square$

The first two assumptions of this lemma are satisfied very commonly, including of course both the case where  $\mathbf{A}_H$  is defined by rediscrretization on the coarse grid and the case of Galerkin coarsening,  $\mathbf{A}_H = (\mathbf{I}_H^h)^T \mathbf{A} \mathbf{I}_H^h$ . The preconditioner  $\mathbf{\Phi}$  is SPD for commonly used MG relaxation methods, including Richardson (where  $\mathbf{\Phi}$  is the identity matrix), Jacobi (where  $\mathbf{\Phi}$  is the inverse of the diagonal of  $\mathbf{A}$ ), and symmetric Gauss-Seidel.

We next adopt the change of variables  $c_{23} = c_2 + c_3$ ,  $\alpha = c_2/c_{23}$ . This yields

$$(3.9) \quad \mathbf{\Gamma} = (1 + c_1)\mathbf{I} - c_{23}\mathbf{W}_\alpha,$$

with

$$(3.10) \quad \mathbf{W}_\alpha = (\alpha\mathbf{\Phi} + (1 - \alpha)\mathbf{I}_H^h \mathbf{A}_H^{-1} \mathbf{I}_h^H) \mathbf{A}.$$

LEMMA 3.2. *The eigenvalues of  $\mathbf{W}_\alpha$  are real and positive for any  $\alpha \in (0, 1]$ .*

*Proof.* This follows from the fact that  $\mathbf{\Phi}$  is SPD, and  $\mathbf{I}_H^h \mathbf{A}_H^{-1} \mathbf{I}_h^H$  is symmetric positive semi-definite. Hence,  $\mathbf{W}_\alpha$  is the product of two SPD matrices and  $\mathbf{S}\mathbf{W}_\alpha\mathbf{S}^{-1}$ , where  $\mathbf{S} = \sqrt{\mathbf{A}}$  as above, is SPD.  $\square$

We henceforth denote the eigenvalues of  $\mathbf{W}_\alpha$  by  $\lambda$ , and assume  $\alpha \in (0, 1]$  (that is,  $c_2$  and  $c_3$  are of the same sign), so the  $\lambda$ 's are all real and positive. We then proceed by fixing  $\alpha$  and optimizing  $c_1$  and  $c_{23}$ . That is, we seek  $c_1$  and  $c_{23}$  which minimize the spectral radius of  $\mathbf{\Upsilon}$ . Under our assumptions, we have  $b \equiv b(c_1, c_{23}, \lambda) = 1 + c_1 - c_{23}\lambda$ , and the worst-case convergence factor is given by:

$$(3.11) \quad \bar{r}(c_1, c_{23}) \triangleq \rho(\mathbf{\Upsilon}) = \max_\lambda |r(c_1, c_{23}, \lambda)|,$$

where  $r = \frac{1}{2}(b \pm \sqrt{b^2 - 4c_1})$ . Per each  $\lambda$ , this quadratic equation obviously has two solutions. Let us denote the absolute value of the solution whose absolute value is the larger of the two by  $\hat{r}$ . Then we can write (3.11) as follows:

$$(3.12) \quad \bar{r}(c_1, c_{23}) = \max_\lambda \hat{r}(c_1, c_{23}, \lambda) \triangleq \frac{1}{2} \left| b + \operatorname{sgn}(b) \sqrt{b^2 - 4c_1} \right|.$$

Here,  $\operatorname{sgn}(\cdot)$  is equal to 1 for non-negative arguments and -1 for negative arguments. Our parameter optimization problem is now defined by

$$(\bar{c}_1, \bar{c}_{23}) = \operatorname{argmin}_{(c_1, c_{23})} \bar{r}(c_1, c_{23}).$$

Interestingly, through the following three lemmas, we can obtain a closed-form solution for the above minimization problem by knowing the maximal and minimal eigenvalues of  $\mathbf{W}_\alpha$ .

LEMMA 3.3.  *$\bar{r}(c_1, c_{23})$  depends only on the maximal and minimal eigenvalues of  $\mathbf{W}_\alpha$ , denoted by  $\lambda_{max}$  and  $\lambda_{min}$ , respectively.*

*Proof.* See Appendix A.  $\square$

LEMMA 3.4. *For any fixed  $c_1$ ,  $\bar{r}(c_1, c_{23})$  is minimized with respect to  $c_{23}$  by choosing it such that  $b(c_1, c_{23}, \lambda_{min}) = -b(c_1, c_{23}, \lambda_{max})$ , and hence  $\hat{r}(c_1, c_{23}, \lambda_{max}) = \hat{r}(c_1, c_{23}, \lambda_{min})$ . The resulting optimal  $c_{23}$  is given by  $c_{23} = 2(1 + c_1)/(\lambda_{max} + \lambda_{min})$ .*

*Proof.* See Appendix B.  $\square$

Plugging the optimal  $c_{23}$  into (3.12) yields

$$(3.13) \quad \bar{r} = \min_{c_1} \frac{1}{2} \left| \mu(1 + c_1) + \sqrt{\mu^2(1 + c_1)^2 - 4c_1} \right|,$$

with

$$\mu = \frac{\kappa - 1}{\kappa + 1},$$

where  $\kappa = \frac{\lambda_{max}}{\lambda_{min}}$  is the condition number of  $\mathbf{W}_\alpha$ . In [Lemma 3.5](#), we determine the optimal  $c_1$ , which minimizes  $\bar{r}$  in [\(3.13\)](#). We assume  $\kappa$  to be strictly greater than 1, so  $\mu \in (0, 1)$ . That is, we omit the trivial case  $\kappa = 1$ , for which convergence occurs in a single iteration with  $c_1 = 0$ .

**LEMMA 3.5.** *The spectral radius  $\bar{r}$  of the iteration matrix is minimized with respect to  $c_1$  by choosing it such that the square-root term in [\(3.13\)](#) vanishes:  $\mu^2(1 + c_1)^2 - 4c_1 = 0$ . This yields*

$$(3.14) \quad c_1^\pm = \frac{2}{\mu^2} - 1 \pm \frac{2}{\mu^2} \sqrt{1 - \mu^2},$$

and the minimizer  $c_1^-$  is the solution with the minus sign before the square-root term.

*Proof.* See [Appendix C](#).  $\square$

To obtain the optimal convergence factor, we substitute  $c_1 = c_1^-$  into [\(3.13\)](#). The worst-case convergence factor with optimal  $c_1$  and  $c_2$  is then given by:

$$\bar{r} = \frac{1}{2}\mu(1 + c_1^-) = \frac{1 - \sqrt{1 - \mu^2}}{\mu}.$$

Recalling that  $\mu = \frac{\kappa - 1}{\kappa + 1}$ , we finally obtain

$$(3.15) \quad \bar{r} = \frac{1 - \sqrt{1 - \mu^2}}{\mu} = \frac{\sqrt{\kappa} - 1}{\sqrt{\kappa} + 1}.$$

We next summary the results of our analysis.

**Summary of Conclusions.** The optimal convergence factor of SESOP-TG with a single history direction, as approximated by our fixed-coefficient analysis, is given by [\(3.15\)](#)

$$\bar{r} = \frac{\sqrt{\kappa} - 1}{\sqrt{\kappa} + 1},$$

where  $\kappa$  is the condition number of  $\mathbf{W}_\alpha$ , optimized over  $\alpha \in (0, 1]$ . This is discussed further below. The optimal coefficient for the history term is given by [\(3.14\)](#) after simplification as

$$(3.16) \quad \bar{c}_1 = \left( \frac{\sqrt{\kappa} - 1}{\sqrt{\kappa} + 1} \right)^2,$$

which is equivalent to the square of the optimal convergence factor indicating that the usage of history will become significant if the problem is ill-posed. The optimal coefficient for the preconditioned gradient terms is given by [\(B.1\)](#) after simplification as

$$(3.17) \quad \bar{c}_{23} = \frac{4}{\lambda_{min}(\sqrt{\kappa} + 1)^2}.$$

These values also apply to classical SESOP without the CGC direction, if we select  $\alpha = 1$  rather than the  $\alpha$  which minimizes the condition number of  $\mathbf{W}_\alpha$ . Finally, the optimal convergence factor for SESOP-TG without the history direction is obtained by setting  $c_1 = 0$ . This yields

$$(3.18) \quad \bar{r} = \frac{\kappa - 1}{\kappa + 1},$$

with the optimal  $c_{23}$  given by

$$(3.19) \quad \bar{c}_{23} = \frac{2}{\lambda_{\min}(\kappa + 1)}.$$

Note the significant improvement provided by the use of history, with the condition number replaced by the square root. These results are reminiscent of the CG method, and indeed there is an equivalence between SESOP and CG for the case of single history and no CGC direction. We note that the condition number in our scheme is the matrix  $\mathbf{W}_\alpha$  not  $\mathbf{A}$  which differs from the case when we do not involve the CGC direction. The advantage of SESOP is in allowing the addition of various directions. The cost is in the requirement to optimize the coefficients. This study is partly aimed at reducing this cost.

**3.1.2. Insights of optimizing the condition number.** The upshot of our analysis thus far is that we should aim to minimize  $\kappa$ , the condition number of  $\mathbf{W}_\alpha$ . In certain cases, particularly when  $\mathbf{A}$  is a circulant matrix (typically the discretization of an elliptic PDE with constant coefficients on a rectangular or infinite domain), this can be done by means of Fourier analysis and we will explain this concern more in [subsection 3.1.3](#). Here we begin with a more general discussion to gain insights into this matter. We consider the case of Galerkin coarsening,  $\mathbf{A}_H = (\mathbf{I}_H^h)^\top \mathbf{A} \mathbf{I}_H^h$  and no preconditioning, i.e.,  $\Phi = \mathbf{I}$ . Following ideas of [7], we assume that the columns of the prolongation matrix  $\mathbf{I}_H^h$  are comprised of a subset of the eigenvectors of  $\mathbf{A}$ .

LEMMA 3.6. *Let  $\eta_i$ ,  $i = 1, \dots, N$ , denote the eigenvalues of  $\mathbf{A}$ , and let  $\mathbf{w}_i$  denote the corresponding eigenvectors. Assume that the columns of the prolongation matrix  $\mathbf{I}_H^h$  are comprised of a subset of the eigenvectors of  $\mathbf{A}$ , and denote by  $\mathcal{R}(\mathbf{I}_H^h)$  the range of the prolongation, that is, the subspace spanned by the columns of  $\mathbf{I}_H^h$ . Denote*

$$\begin{aligned} \eta_{fmax} &= \max_{i:\mathbf{w}_i \notin \mathcal{R}(\mathbf{I}_H^h)} \eta_i, & \eta_{fmin} &= \min_{i:\mathbf{w}_i \notin \mathcal{R}(\mathbf{I}_H^h)} \eta_i, \\ \eta_{cmax} &= \max_{i:\mathbf{w}_i \in \mathcal{R}(\mathbf{I}_H^h)} \eta_i, & \eta_{cmin} &= \min_{i:\mathbf{w}_i \in \mathcal{R}(\mathbf{I}_H^h)} \eta_i. \end{aligned}$$

Then, the condition number of  $\mathbf{W}_\alpha$  in (3.10) with  $\Phi = \mathbf{I}$  is given by

$$(3.20) \quad \kappa = \frac{\max(\alpha\eta_{fmax}, \alpha\eta_{cmax} + 1 - \alpha)}{\min(\alpha\eta_{fmin}, \alpha\eta_{cmin} + 1 - \alpha)}.$$

*Proof.* Any eigenvector  $\mathbf{w}_i \in \mathcal{R}(\mathbf{I}_H^h)$  (respectively,  $\mathbf{w}_i \notin \mathcal{R}(\mathbf{I}_H^h)$ ) is an eigenvector of the CGC matrix  $\mathbf{I}_H^h \mathbf{A}_H^{-1} (\mathbf{I}_H^h)^\top \mathbf{A}$ , with eigenvalue 1 (respectively, 0), because if  $\mathbf{w}_i \in \mathcal{R}(\mathbf{I}_H^h)$  then it can be written as  $\mathbf{w}_i = \mathbf{I}_H^h \mathbf{e}_j$  (that is, it is the  $j$ th column for some  $j$ ), so

$$[\mathbf{I}_H^h \mathbf{A}_H^{-1} (\mathbf{I}_H^h)^\top \mathbf{A}] \mathbf{w}_i = \mathbf{I}_H^h [(\mathbf{I}_H^h)^\top \mathbf{A} \mathbf{I}_H^h]^{-1} [(\mathbf{I}_H^h)^\top \mathbf{A} \mathbf{I}_H^h] \mathbf{e}_j = \mathbf{I}_H^h \mathbf{e}_j = \mathbf{w}_i,$$

whereas if  $\mathbf{w}_i \notin \mathcal{R}(\mathbf{I}_H^h)$  then it is orthogonal to the columns of  $\mathbf{I}_H^h$ , so

$$[\mathbf{I}_H^h \mathbf{A}_H^{-1} (\mathbf{I}_H^h)^\top \mathbf{A}] \mathbf{w}_i = [\mathbf{I}_H^h \mathbf{A}_H^{-1} (\mathbf{I}_H^h)^\top] \eta_i \mathbf{w}_i = \mathbf{0}.$$

It follows that the eigenvectors of  $\mathbf{W}_\alpha$  are  $\mathbf{w}_i$ , with eigenvalues given by

$$\lambda_i = \begin{cases} \alpha\eta_i + 1 - \alpha & \text{if } \mathbf{w}_i \in \mathcal{R}(\mathbf{I}_H^h), \\ \alpha\eta_i & \text{otherwise} \end{cases}$$

The proof follows.  $\square$

We see that the second term in  $\mathbf{W}_\alpha$ , which corresponds to the direction given by the CGC, increases the eigenvalues associated with the columns of the prolongation by  $1 - \alpha$ . It thus follows from (3.20) that, to obtain any advantage at all from the coarse-grid direction in reducing  $\kappa$ , the eigenvector associated with the smallest  $\eta_i$  must be included amongst the columns of the prolongation, and therefore  $\eta_{cmin} \leq \eta_{fmin}$ . Similarly, considering the numerator in (3.20), it is clearly advantageous that the eigenvector corresponding to the largest  $\eta_i$  not be included in the range of the prolongation. With these assumptions, we can make the following observation.

**THEOREM 3.7.** *Assume  $\eta_{cmin} \leq \eta_{fmin}$  and  $\eta_{cmax} \leq \eta_{fmax}$ . Then the condition number  $\kappa$  is minimized for*

$$\alpha = \alpha_{opt} = \frac{1}{1 + \eta_{fmin} - \eta_{cmin}} \leq 1,$$

and the resulting optimal  $\kappa$  is given by

$$(3.21) \quad \kappa = \kappa_{opt} = \begin{cases} \frac{\eta_{fmax}}{\eta_{fmin}} & \text{if } \eta_{fmax} - \eta_{fmin} \geq \eta_{cmax} - \eta_{cmin}, \\ 1 + \frac{\eta_{cmax} - \eta_{cmin}}{\eta_{fmin}} & \text{otherwise} \end{cases}$$

*Proof.* Note that  $\alpha_{opt}$  is nothing but the value of  $\alpha$  for which  $\alpha\eta_{fmin} = \alpha\eta_{cmin} + 1 - \alpha$  in the denominator in (3.20). Denote also by  $\alpha_{top} = \frac{1}{1 + \eta_{fmax} - \eta_{cmax}} \leq 1$  the value of  $\alpha$  for which  $\alpha\eta_{fmax} = \alpha\eta_{cmax} + 1 - \alpha$  in the numerator in (3.20). It is evident from (3.20) that  $\kappa$  is bounded from below by  $\eta_{fmax}/\eta_{fmin}$ . This bound can be realized when  $\eta_{fmax} - \eta_{fmin} \geq \eta_{cmax} - \eta_{cmin}$ . In this case,  $\alpha_{top} \leq \alpha_{opt}$ , and the bound is realized by selecting any  $\alpha$  in the range  $\alpha \in [\alpha_{top}, \alpha_{opt}]$ , because the numerator is then maximized by  $\alpha\eta_{fmax}$ , while the denominator is minimized by  $\alpha\eta_{fmin}$ .

When  $\eta_{fmax} - \eta_{fmin} < \eta_{cmax} - \eta_{cmin}$ , we can no longer match the lower bound. In this case  $\alpha_{top} > \alpha_{opt}$  and we have three regimes:

1.  $0 < \alpha < \alpha_{opt} \Rightarrow \kappa = \frac{\alpha\eta_{cmax} + 1 - \alpha}{\alpha\eta_{fmin}}$ ,  $\frac{d\kappa}{d\alpha} = -\frac{1}{\alpha^2\eta_{fmin}} < 0$ .
2.  $\alpha_{opt} < \alpha < \alpha_{top} \Rightarrow \kappa = \frac{\alpha\eta_{cmax} + 1 - \alpha}{\alpha\eta_{cmin} + 1 - \alpha}$ ,  $\frac{d\kappa}{d\alpha} = \frac{\eta_{cmax} - \eta_{cmin}}{(\alpha\eta_{cmin} + 1 - \alpha)^2} > 0$ .
3.  $\alpha_{top} < \alpha < 1 \Rightarrow \kappa = \frac{\alpha\eta_{fmax}}{\alpha\eta_{cmin} + 1 - \alpha}$ ,  $\frac{d\kappa}{d\alpha} = \frac{\eta_{fmax}}{(\alpha\eta_{cmin} + 1 - \alpha)^2} > 0$ .

We find that  $\kappa$  decreases monotonically for  $\alpha < \alpha_{opt}$  and increases monotonically for  $\alpha > \alpha_{opt}$ , so  $\alpha_{opt}$  is indeed the minimizer. Substitution into (3.20) completes the proof.  $\square$

**Discussion.** Examining (3.21), we find that  $\kappa_{opt}$  is either equal to  $\eta_{fmax}/\eta_{fmin}$ , or else it is only “slightly larger”, because

$$1 + \frac{\eta_{cmax} - \eta_{cmin}}{\eta_{fmin}} = \frac{\eta_{fmax}}{\eta_{fmin}} + 1 - \frac{\eta_{fmax} - \eta_{cmax} + \eta_{cmin}}{\eta_{fmin}} < \frac{\eta_{fmax}}{\eta_{fmin}} + 1.$$

That is, even in the regime  $\eta_{fmax} - \eta_{fmin} < \eta_{cmax} - \eta_{cmin}$ , the optimal condition number  $\kappa_{opt}$  is increased by less than 1. Observe that  $\kappa = \eta_{fmax}/\eta_{fmin}$  yields a convergence factor (with no history) of  $\mu = \frac{\kappa - 1}{\kappa + 1}$ , which matches that of the classical Two-Grid algorithm with optimally weighted Richardson relaxation followed by CGC. Indeed, our numerical tests with a variety of problems and algorithm details usually show a good agreement between SESOP-TG with no history and the classical Two-Grid algorithm with optimal weighting of the relaxation and CGC. Of course, adding history improves the convergence factors. Finally, observe that the optimal prolongation is obtained by choosing the columns of  $I_H^h$  to be the eigenvectors associated with the smallest eigenvalues of  $\mathbf{A}$  (similarly to the classical Two-Grid case

[7]). This clearly minimizes the ratio  $\eta_{fmax}/\eta_{fmin}$ . Furthermore, this choice yields  $\eta_{cmax} \leq \eta_{fmin}$ , so even if  $\eta_{fmax} - \eta_{fmin} < \eta_{cmax} - \eta_{cmin}$  (so  $\kappa_{opt} > \eta_{fmax}/\eta_{fmin}$ ), we obtain  $\kappa_{opt} = 1 + \frac{\eta_{cmax} - \eta_{cmin}}{\eta_{fmin}} < 2$ .

**3.1.3. Optimizing the condition number in practice.** According to the previous analyses, we know if we only have three directions, namely one history, gradient (may have preconditioner), CGC, in the subspace, there exist fixed coefficients for these three directions to yield an optimal asymptotic convergence factor for linear problems. We already know the optimal convergence factor is governed by  $\kappa$ , the condition number of  $\mathbf{W}_\alpha$ . So finding an optimal  $\alpha$  to minimize  $\kappa$  is a crucial step to yield optimal convergence factor and to obtain the corresponding fixed stepsizes. However, in general, minimizing  $\kappa$  needs high complexity since evaluating the condition number of a given matrix one time is already very high. Moreover, the assumptions shown in subsection 3.1.2 are only valid for some special examples which limits the usage of these results. In this part, we show that optimizing  $\kappa$  will become easily if  $\mathbf{A}$  is formulated from an elliptic PDE with constant coefficients that local Fourier analysis can be applied.

We already know local Fourier Analysis, or called local mode analysis, is a very useful quantitative tool for estimating the asymptotic convergence factor of MG methods for solving elliptic PDEs with constant coefficients [2, 22]. With the help of Fourier analysis, the eigenvalues of  $\mathbf{W}_\alpha$  can be obtained easily then evaluating  $\kappa$  becomes cheap. So we can just apply a line search method to finding the optimal  $\alpha$  with low complexity. Without loss of generality, we show a two dimensional case and without the preconditioner. Denote by  $L_h$  the elliptic operator with equal mesh-size  $h$ . Clearly, the grid functions  $\psi(\boldsymbol{\theta}, x, y) = e^{\iota\theta_1 x/h} e^{\iota\theta_2 y/h}$  with  $\boldsymbol{\theta} = (\theta_1, \theta_2) \in [-\pi, \pi]^2$  and  $\iota = \sqrt{-1}$  are the eigenfunctions of  $L_h$ , i.e.,  $L_h \psi(\boldsymbol{\theta}, x, y) = \tilde{L}_h(\boldsymbol{\theta}) \psi(\boldsymbol{\theta}, x, y)$  with  $\tilde{L}_h(\boldsymbol{\theta}) = \sum_{\mathbf{k}} a_{\mathbf{k}} e^{\iota\boldsymbol{\theta} \cdot \mathbf{k}}$  and  $\tilde{L}_h(\boldsymbol{\theta})$  is called the formal eigenvalue or the symbol of  $L_h$ .  $\{a_{\mathbf{k}}\}$  are the corresponding constant coefficients in  $L_h$  with  $\mathbf{k} = (k_1, k_2)$  and we utilize  $\cdot$  to denote the element-wise product when we represent  $\tilde{L}_h(\boldsymbol{\theta})$ . Obviously, all of the grid functions consist of the eigenvectors of  $\mathbf{A}$  and the eigenvalues of  $\mathbf{A}$  are specified by  $\tilde{L}_h(\boldsymbol{\theta})$ .

Reminding  $\mathbf{W}_\alpha = \alpha \mathbf{A} + (1 - \alpha) \mathbf{I}_H^h \mathbf{A}_H^{-1} \mathbf{I}_h^H \mathbf{A}$  without any preconditioner (cf. (3.10)) and the typical two-grid Fourier analysis formulation in MG methods [22], we know the eigenvalues of  $\mathbf{W}_\alpha$  are equivalent to the eigenvalues of the following  $4 \times 4$  matrix with going over the whole  $(\theta_1, \theta_2) \in T^{low}$  domain:

$$\begin{aligned}
 \tilde{\mathbf{W}}_\alpha^{\theta_1, \theta_2} &= \alpha \tilde{\mathbf{A}}^{\theta_1, \theta_2} + (1 - \alpha) \left( \tilde{\mathbf{I}}_H^h \right)^{\theta_1, \theta_2} \left( \tilde{\mathbf{A}}_H^{\theta_1, \theta_2} \right)^{-1} \left( \tilde{\mathbf{I}}_h^H \right)^{\theta_1, \theta_2} \tilde{\mathbf{A}}^{\theta_1, \theta_2} \\
 \tilde{\mathbf{A}}^{\theta_1, \theta_2} &= \begin{bmatrix} \tilde{L}_h(\theta_1, \theta_2) & & & \\ & \tilde{L}_h(\bar{\theta}_1, \theta_2) & & \\ & & \tilde{L}_h(\theta_1, \bar{\theta}_2) & \\ & & & \tilde{L}_h(\bar{\theta}_1, \bar{\theta}_2) \end{bmatrix} \\
 \tilde{\mathbf{A}}_H^{\theta_1, \theta_2} &= \frac{1}{4} \tilde{L}_h(2\theta_1, 2\theta_2) - \text{rediscretization} \\
 &\text{or} \\
 \tilde{\mathbf{A}}_H^{\theta_1, \theta_2} &= \left( \tilde{\mathbf{I}}_h^H \right)^{\theta_1, \theta_2} \tilde{L}_h(2\theta_1, 2\theta_2) \left( \tilde{\mathbf{I}}_H^h \right)^{\theta_1, \theta_2} - \text{Galerkin form} \\
 \bar{\theta}_i &= \begin{cases} \theta_i + \pi, & \text{if } \theta_i < 0 \\ \theta_i - \pi, & \text{if } \theta_i > 0 \end{cases}, \quad i = 1, 2
 \end{aligned}
 \tag{3.22}$$

where  $\left( \tilde{\mathbf{I}}_H^h \right)^{\theta_1, \theta_2} \in \mathfrak{R}^{4 \times 1}$  and  $\left( \tilde{\mathbf{I}}_h^H \right)^{\theta_1, \theta_2} \in \mathfrak{R}^{1 \times 4}$  denote the symbols of the prolongation and restriction, respectively. Note that the definition of  $T^{low}$  is proposed in

**Definition 3.8** and we omit the trivial angles that any element in  $\tilde{\mathbf{A}}^{\theta_1, \theta_2}$  or  $\tilde{\mathbf{A}}_H^{\theta_1, \theta_2}$  is zero in practice. From this viewpoint, we transform the calculation of the eigenvalues of  $\mathbf{W}_\alpha$  from its original form to a series of matrices, i.e.,  $\tilde{\mathbf{W}}_\alpha^{\theta_1, \theta_2}$  for all  $\boldsymbol{\theta} \in T^{low}$ . Thus, evaluating the condition number of  $\mathbf{W}_\alpha$  becomes cheap so that we can utilize a line search method to find  $\alpha$  for minimizing  $\kappa$ . In the numerical experiments, we show the effectiveness of such a method.

DEFINITION 3.8 (low and high frequencies).

$$\begin{aligned} \tilde{L}_h(\boldsymbol{\theta}) \text{ is low frequency component} &\iff \boldsymbol{\theta} \in T^{low} := \left[-\frac{\pi}{2}, \frac{\pi}{2}\right)^2, \\ \tilde{L}_h(\boldsymbol{\theta}) \text{ is high frequency component} &\iff \boldsymbol{\theta} \in T^{high} := [-\pi, \pi)^2 \setminus \left[-\frac{\pi}{2}, \frac{\pi}{2}\right)^2. \end{aligned}$$

**3.1.4. Ideal MG methods.** With the definitions of high and low frequencies in **Definition 3.8**, we say the MG method is ideal if it only eliminates the high frequency components efficiently on the fine-grid and smooth the low frequency components on the coarse-grid then the ideal MG method yields  $\eta_{fmax} = \max_{\boldsymbol{\theta} \in T^{high}} \tilde{L}_h(\boldsymbol{\theta})$  and  $\eta_{fmin} = \min_{\boldsymbol{\theta} \in T^{high}} \tilde{L}_h(\boldsymbol{\theta})$  and  $\kappa_{opt}$  of the ideal convergence factor for SESOP-TG with one history is  $\frac{\sqrt{\kappa_{opt}}-1}{\sqrt{\kappa_{opt}}+1}$  with  $\kappa_{opt} = \frac{\eta_{fmax}}{\eta_{fmin}}$ . Here, we omit the another solution of  $\kappa_{opt}$  shown in **subsection 3.1.2** since we are interested in considering ill-conditioned problems. In the numerical experiments, we will see such an ideal convergence factor is achievable.

**The connection with  $h$ -ellipticity measure.**  $h$ -ellipticity measure,  $E_h(L_h)$ , is a quantitative measure of ellipticity of a discrete operator and is defined in **Definition 3.9** [20]. For an ill-posed problem, an ideal MG method should yield  $\kappa_{opt} = \frac{1}{E_h}$ . Representing the ideal convergence factor with the  $h$ -ellipticity measure of our scheme yields  $r = \frac{1-\sqrt{E_h}}{1+\sqrt{E_h}}$ . Typically, if using history is not allowed, the convergence factor becomes  $\frac{1-E_h}{1+E_h}$  which is the well known rate for the case when the optimally damped Jacobi method is chosen as the relaxation [20]. Clearly, a large  $E_h$  means a well-posed problem.

DEFINITION 3.9. *The  $h$ -ellipticity measure  $E_h$  of  $L_h$  is defined as*

$$E_h(L_h) := \frac{\min\{|\tilde{L}_h(\boldsymbol{\theta})| : \boldsymbol{\theta} \in T^{high}\}}{\max\{|\tilde{L}_h(\boldsymbol{\theta})| : \boldsymbol{\theta} \in T^{high}\}}$$

where  $\tilde{L}_h(\boldsymbol{\theta})$  represents the Fourier symbol of  $L_h$ .

**3.2. Multilevel version – SESOP-MG.** Now, we extend our SESOP-TG method to multilevels, called SESOP-MG, for practical usage. In multilevel version, we solve the coarse problem recursively to reduce the computation. Specifically, SESOP-MG is obtained via replacing Step 4 in **Algorithm 3.1** by **Algorithm 3.2**. Clearly, we retain the V-cycle by setting *CycleType* = 1 and obtain the W-cycle by setting *CycleType* = 2 and call **Algorithm 3.2** two times. Moreover, one can also combine our scheme with F-cycle to obtain a good initial value and then call V-cycle to save the whole computation which is not shown in this paper [5]. In following experiments, we utilize random initialization.

**4. Experimental results.** We investigate the performance of our approach for solving linear and nonlinear problems in this section. For the linear problem, we mainly focus on the rotated anisotropic diffusion problem. To clearly demonstrate the potential of the proposed approach and examine the relevance of the above theoretic

**Algorithm 3.2** SESOP-MG: Coarse Solver

---

```

1: function  $\mathbf{x}_l^* = \dots$ 
   SESOP_MG_CoarseSolver( $\mathbf{x}_{l,k}, \nabla\sigma_{l-1,k}(\mathbf{x}_{l-1,k}), L, v_1, v_2, CycleType$ ) %  $l > 1$ .
2:  $\mathbf{x}_{l,k} \leftarrow Relaxation(\mathbf{x}_{l,k}, v_1)$  % Prerelaxation
3: Construct  $\sigma_{l,k}(\mathbf{x}_l) = \mathcal{F}_{l,k}(\mathbf{x}_l) - \mathbf{v}_{l,k}^T \mathbf{x}_l$  where  $\mathbf{v}_l = \nabla \mathcal{F}_{l,k}(\mathbf{x}_{l,k}) - I_h^H \nabla \sigma_{l-1,k}(\mathbf{x}_{l-1,k})$ 
4: Calculate  $\nabla \sigma_{l,k}(\mathbf{x}_{l,k})$  and formulate the subspace
    $\mathbf{P}_k \leftarrow \nabla \sigma_{l,k}(\mathbf{x}_{l,k})$ 
5: if  $l < L$  then
6:    $\mathbf{x}_{l+1,k} \leftarrow I_h^H \mathbf{x}_{l,k}$ 
7:   % Solve  $(l+1)$ th level problem through recursive
8:    $\mathbf{x}_{l+1}^* \leftarrow \mathbf{x}_{l+1,k}$ 
9:    $CycleNum \leftarrow 1$ 
10:  for  $CycleNum \leq CycleType$  do
11:     $\mathbf{x}_{l+1}^* \leftarrow SESOP\_MG\_CoarseSolver(\mathbf{x}_{l+1}^*, \nabla \sigma_{l,k}(\mathbf{x}_{l,k}), L, v_1, v_2, CycleType)$ 
12:     $CycleNum \leftarrow CycleNum + 1$ 
13:  end for
14:  % add coarse correction into the subspace
15:  Formulate the coarse correction  $I_H^h (\mathbf{x}_{l+1}^* - \mathbf{x}_{l+1,k})$  to obtain
    $\bar{\mathbf{P}}_k \leftarrow [I_H^h (\mathbf{x}_{l+1}^* - \mathbf{x}_{l+1,k}) \quad \mathbf{P}_k]$ .
16: else
17:    $\bar{\mathbf{P}}_k \leftarrow \mathbf{P}_k$ 
18: end if
19: Solve  $\alpha_k = \operatorname{argmin}_{\alpha} \sigma_{l,k}(\mathbf{x}_{l,k} + \bar{\mathbf{P}}_k \alpha)$  and then  $\mathbf{x}_{l,k} \leftarrow \mathbf{x}_{l,k} + \bar{\mathbf{P}}_k \alpha_k$ 
20:  $\mathbf{x}_{l,k} \leftarrow Relaxation(\mathbf{x}_{l,k}, v_2)$  % Postrelaxation
21: return  $\mathbf{x}_l^* \leftarrow \mathbf{x}_{l,k}$ 

```

---

analyses coincide with practical situations, we apply our scheme to a two-level setting of the linear problem first, that is to say the hierarchy is comprised of only two-level: the original problem and just one coarser-level. Then we show the difference of the convergence factor either we recalculate the stepsizes in each iteration through subspace minimization or utilize the results shown in [subsection 3.1.3](#) to obtain the fixed stepsizes. Note that we conduct such a comparison on a two-level setting. After these, we extend the two-level to multilevels which we called SESOP-MG to see the practical performance further. Moreover, we compare our SESOP-MG with the preconditioned conjugate gradient (PCG) which utilizes a standard MG method as the preconditioner. The standard MG method here means we utilize the Jacobi method with optimally damped factor as the relaxation with a CGC. The numerical experiments demonstrate the efficiency of our method. For the nonlinear problems, we apply the multilevel version of our framework to exploring its performance further. Moreover, we also compare our approach with the steepest descent (SD), Nesterov's acceleration method [15], and limited-memory BFGS (LBFGS) [24] for the nonlinear problems. In this part, we utilize "MG" to denote a MG method which utilizes the steepest method as the relaxation and exploits a line search method to find a suitable stepsize for the CGC.

**4.1. Solving the rotated anisotropic diffusion problem.** The rotated anisotropic diffusion problem is described as follows:

$$(4.1) \quad \mathcal{L}u = f,$$

where  $\mathcal{L}u = u_{ss} + \epsilon u_{tt}$ , with  $u_{ss}$  and  $u_{tt}$  denoting the second partial derivatives of  $u$  in the  $(s, t)$  coordinate system. Representing (4.1) in the  $(x, y)$  coordinate system, this leads

$$(4.2) \quad \mathcal{L}u = (C^2 + \epsilon S^2)u_{xx} + 2(1 - \epsilon)CSu_{xy} + (\epsilon C^2 + S^2)u_{yy},$$

where  $C = \cos \phi$  and  $S = \sin \phi$  with  $\phi$  the angle between  $(s, t)$  and  $(x, y)$ . The discretization of (4.2) with mesh-size  $h$  is

$$(4.3) \quad \mathcal{L}^h \otimes \mathbf{u}^h = \mathbf{f}^h,$$

where  $\otimes$  denotes the convolutional operator,

$$\mathcal{L}^h = \frac{1}{h^2} \begin{bmatrix} -\frac{1}{2}(1 - \epsilon)CS & \epsilon C^2 + S^2 & \frac{1}{2}(1 - \epsilon)CS \\ C^2 + \epsilon S^2 & -2(1 + \epsilon) & C^2 + \epsilon S^2 \\ \frac{1}{2}(1 - \epsilon)CS & \epsilon C^2 + S^2 & -\frac{1}{2}(1 - \epsilon)CS \end{bmatrix},$$

and  $\mathbf{u}^h, \mathbf{f}^h$  are the discretization of  $u$  and  $f$  on the fine grid, respectively. Note that the coarse problem is formulated through rediscrizing (4.1) with mesh-size  $2h$ .

Denote by SESOP-TG- $i$  the SESOP-TG with  $i$  histories. Similarly, we utilize SESOP-MG- $i$  to denote the multilevel version with  $i$  histories. Without any special mention, we solve (4.3) on a  $64 \times 64$  grids with Dirichlet boundary condition and the restriction and prolongation are set to be the full weighting and bilinear. Moreover, we choose the Jacobi method with optimally damped factor as the relaxation.

Firstly, we verify whether our theoretic prediction of the asymptotic convergence factor for a given fixed stepsizes matches the practical case. Note that we do not pursue a fastest convergence factor in this experiment. So we set  $c_3 = 1$  and  $\kappa = \frac{1}{E_h(\mathcal{L}^h)}$  with  $\lambda_{min}$  the numerator of  $E_h(\mathcal{L}^h)$ . Then we utilize (3.16) and (3.17) to obtain  $c_1$  and  $c_2$ . Although the fixed stepsizes are used here to instead of the subspace minimization, we still call it SESOP-TG-1 in this experiment. With the given fixed stepzies, we run SESOP-TG-1 until the residual norm, defined as  $\|\mathcal{L}^h \mathbf{u}_k^h - \mathbf{f}^h\|_F$ , is smaller than  $10^{-8}$ . After this, the practical convergence factor is calculated via

$$\sqrt[10]{\frac{\|\mathcal{L}^h \mathbf{u}_{Iter_{final}}^h - \mathbf{f}^h\|_F}{\|\mathcal{L}^h \mathbf{u}_{Iter_{final}-10}^h - \mathbf{f}^h\|_F}},$$

where  $Iter_{final}$  denotes the total number of iterations when SESOP-TG-1 is convergent. We test SESOP-TG-1 on various  $\epsilon$  and  $\phi$  to check the accuracy of our theoretic predictions. Observing from Figure 1, we see the analytic predictions perfectly match the practical ones for various  $\epsilon$  and  $\phi$  demonstrating the accuracy of our theoretic predictions.

Secondly, we choose the stepsizes through the subspace minimization for SESOP-TG-1 to compare its performance with SESOP-TG-0 and TG. From Figures 2(a) and 2(c), we observe that SESOP-TG-1 converges fastest in decreasing the residual norm than SESOP-TG-0 and TG illustrating the promising performance of using history. Moreover, we also compare the asymptotic convergence factor of these three methods versus cycles, see Figures 2(b) and 2(d). Obviously, SESOP-TG-1 yields a smallest convergence factor than other two methods. Without any confusion, we utilize iteration and cycle interchangeably in this paper. Moreover, we also compare the convergence factor of the practical cases with the ideal one, defined by  $\frac{1 - \sqrt{E_h}}{1 + \sqrt{E_h}}$ , to

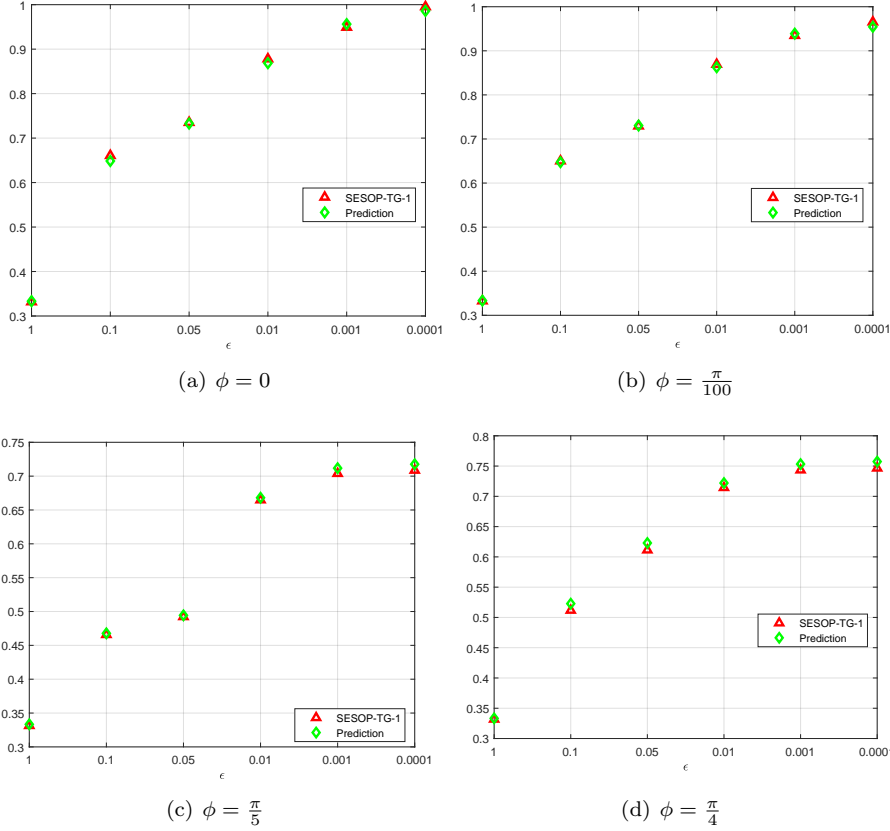


FIG. 1. The comparison of the asymptotic convergence factor between the theoretic predictions and practical cases for SESOP-TG-1 with various  $\phi$  and  $\epsilon$ .

see their difference. From Table 1, we notice the convergence factor of the practical cases meet the ideal predictions when  $\epsilon = 1$  and  $\phi = 0$ . However, for  $\epsilon = 10^{-3}$  and  $\phi = \frac{\pi}{4}$ , the practical convergence factors become worse than the ideal one because, in general, we cannot guarantee only high frequency is erased on the fine-grid and the low frequency is smoothed on the coarse-grid. Moreover, the prolongation is also not an ideal one, see Lemma 3.6 and [11].

TABLE 1

The Comparison of convergence factor between Ideal and practical cases. Left: ideal cases; right: practical cases.

$\epsilon$	$\phi$	TG		SESOP-TG-0		SESOP-TG-1	
1	0	0.600	0.594	0.600	0.600	0.333	0.333
$10^{-3}$	$\frac{\pi}{4}$	0.744	0.738	0.744	0.790	0.446	0.503

Thirdly, we investigate the performance of our scheme when determines the step-sizes through minimizing the  $\kappa$  by utilizing the results shown in subsections 3.1.1 and 3.1.3 which we call the optimized one. The purpose of this experiment is to see whether using the fixed stepsizes scheme can achieve the similar performance as the one which calculates the stepsizes through subspace minimization. Note that

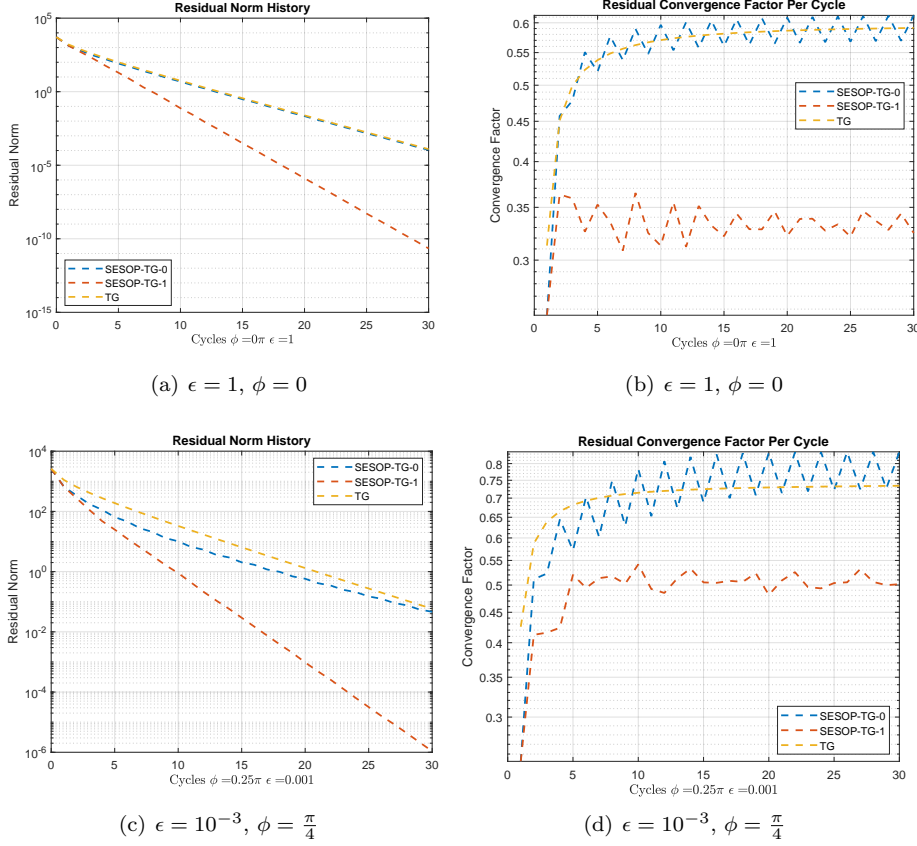


FIG. 2. Residual norm and convergence factor versus cycles with different  $\epsilon$  and  $\phi$  for the rotated anisotropic problem.

the problem in this example is linear so that we solve the subspace problem exactly. The restriction is still the full weighting, but both the bilinear and bicubic prolongations are considered here to see their difference. Note that if we can smooth the low-frequency efficiency by setting  $c_3 = 1$ , the strategy of determining the stepsizes shown in Figure 1 is already an optimal one. So we also add this strategy of choosing the stepsizes in this comparison referring to the ordinary one.

From Table 2, we clearly observe that the optimized one yields a better convergence factor than the ordinary one that we do not optimize  $\kappa$ . Moreover, we notice that the optimized one yields a similar convergence factor as SESOP which calculates the stepsizes through subspace minimization. This implies the robustness of our scheme and indicates that choosing the stepsizes locally can still lead to an acceptable convergence factor. However, if the optimized stepsizes is known, we can avoid the subspace minimization to save computation which can be seen in the next experiment. We also observe the bicubic prolongation yields a better convergence factor than the bilinear satisfying the expectation [11]. Excluding the case when  $\epsilon = 1$  and  $\phi = 0$ , we notice that the convergence factors in the ordinary one are much worse than the ideal one, especially  $\phi = \frac{\pi}{4}$ , which is reasonable because setting  $c_3 = 1$  cannot always effectively smooth the low frequency modes. Note that choosing the bicubic prolon-

gation results in a slightly better convergence factor than the ideal one illustrating the effectiveness of optimizing  $\kappa$  in practice.

TABLE 2

The Comparison of the convergence factor among the ordinary one (Ord.), the subspace minimization one (SESOP), and the optimized one (Opt.) for determining the stepsizes. The Ideal one ( $h$ -ellipticity measure) is added as a benchmark. Note that the periodic boundary condition is set for the SESOP one in this example.

$\phi$	$\epsilon$	Bilinear			Bicubic			Ideal One
		Ord.	SESOP	Opt.	Ord.	SESOP	Opt.	
0	1	0.333	0.332	0.332	0.333	0.333	0.331	0.333
$\frac{\pi}{6}$	$10^{-3}$	0.669	0.570	0.563	0.587	0.537	0.532	0.587
$\frac{\pi}{6}$	$10^{-4}$	0.676	0.572	0.565	0.588	0.538	0.533	0.588
$\frac{\pi}{4}$	$10^{-3}$	0.753	0.509	0.500	0.653	0.457	0.443	0.446
$\frac{\pi}{4}$	$10^{-4}$	0.757	0.511	0.502	0.658	0.458	0.445	0.446

We have shown the coincidence of our analyses and practical cases (cf. Figure 1) and the advantage of our scheme in two-grid version (cf. Table 1 and Figure 2). Moreover, we also show the merits of optimizing  $\kappa$  for  $\mathbf{W}_\alpha$  (cf. Table 2). Now, we extend the two-grid case to multilevels to see its practical performance for solving the rotated anisotropic problem. We utilize the method shown in subsection 3.1.3 to determine the stepsizes through minimizing  $\kappa$  to avoid the subspace minimization. To save the computation of obtaining  $\alpha$  further, we calculate the optimal  $\alpha$  on a smaller number of grids rather than the problem which we want to solve, e.g., we want to solve the problem on  $1024 \times 1024$  grids but we may determine the  $\alpha$  on  $64 \times 64$  grids. Denote by  $r_{Num}^{opt}$  the convergence factor of optimizing  $\kappa$  on  $Num \times Num$  grids. Then we define

$$r_{ratio}(Num) \triangleq \frac{\log r_{1024}^{opt}}{\log r_{Num}^{opt}} - 1$$

to measure the deterioration of the convergence factor by using the above strategy to determine  $\alpha$ . In Figure 3, we show the difference of  $r_{ratio}(Num)$  for various  $\epsilon$  and  $\phi$  with  $Num = 16, 32, 64, 128, 256, 512$ . Clearly, we see  $r_{ratio}(Num)$  is smaller than 0.1 when  $Num \geq 128$  which means, compared with optimizing the fixed stepsizes on a true grid, determining the stepsizes on  $128 \times 128$  grids needs 10% additional computation. However, in the following experiment, we show such a deterioration is acceptable.

To demonstrate the effectiveness of such a strategy, we compare the SESOP-MG method with 1 history, denoted by SESOP-MG-1, to the PCG method with the standard MG method as the preconditioner and the one which we utilize optimal fixed stepsizes, denoted as SESOP-MG-1-Fixed for solving the rotated anisotropic problem. Notice that we only show the two-grid analysis in subsection 3.1.3 which assuming the coarse problem is solved exactly. To achieve this in practice, we set  $v_1 = 2$  and  $v_2 = 1$  for coarse problems on each level and utilize W-cycle. We note that if one prefers to utilize V-cycle and less number of pre- and postrelaxation in practice, the three-grid analysis can be introduced to replace the two-grid analysis shown in subsection 3.1.3 to determine  $\alpha$  as the three-grid analysis matches the property of the multilevel version better [23].

We conduct the experiments in this part on a laptop with Intel (R) i7-6500U 2.5GHz CPU. Note that we determine the stepsizes for SESOP-MG-1-Fixed on  $64 \times 64$  grids, needing almost 1.5 seconds in practice, but solve the problem on  $1024 \times 1024$ .

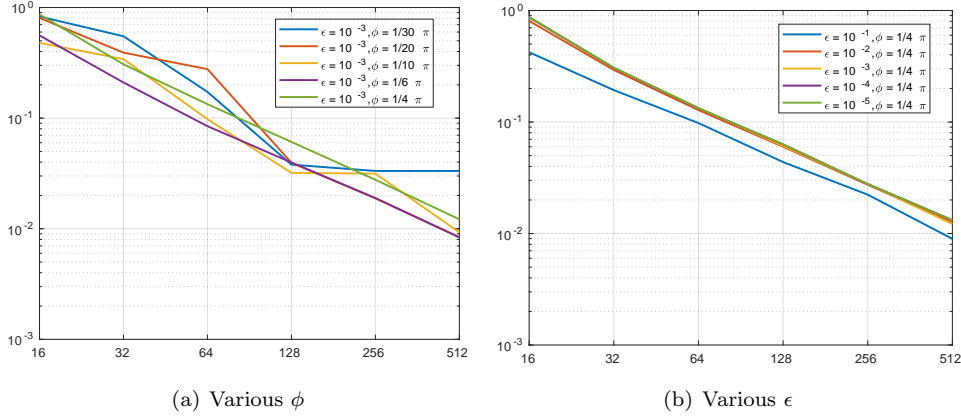


FIG. 3. The difference of  $r_{deter}(Num)$  for determining the stepsizes between smaller number of grids and the true number of grids, i.e.,  $1024 \times 1024$ , for different  $\epsilon$  and  $\phi$ .

As shown in Figure 4(a), we find SESOP-MG-1 works almost the same as PCG with the standard MG as the preconditioner. Moreover, we also see SESOP-MG-1-Fixed works as good as the SESOP-MG-1 and PCG-MG even we determine the stepsizes on a small number of grids. Observing from Figure 4(c), we find SESOP-MG-1 becomes better than PCG when  $\phi = 10^{-3}$  and  $\phi = \frac{\pi}{4}$  because the standard MG does not work efficiently enough in this example. In practice, we have to overweight the residual when we go to coarse to retain the efficiency of the standard MG in this case [4]. However, SESOP-MG-1-Fixed and SESOP-MG-1 do not suffer from such a problem as they determine the stepsizes through minimizing  $\kappa$  and subspace minimization, respectively. From Figures 4(b) and 4(d), we clearly see SESOP-MG-1-Fixed is even faster than PCG in terms of CPU time which is reasonable because PCG needs more computation in each iteration. Interestingly, we see SESOP-MG-1-Fixed even needs less CPU time than the standard MG method because, excluding the relaxation, the standard MG needs to evaluate the gradient one more time for calculating the residual, but, in SESOP-MG-1-Fixed, we also add this in the subspace for further utilizing.

**4.2. Solving nonlinear problems.** Two nonlinear problems are considered in this section to show the efficiency of our approach for solving large-scale problems further. The full weighting restriction and bilinear prolongation are chosen here. In this part, the steepest descent (SD) method is chosen as the relaxation for MG [21] and SESOP-MG. The number of pre- and postrelaxation for MG and SESOP-MG is set to be 1 and 0, respectively. Note that we utilize the BFGS method, the maximal number of iterations is set to be 10, to solve the coarsest problem and the Newton method to address the subspace minimization problem both through the minFunc toolbox [17]. All of the experiments in this part are conducted on a work station with an Intel(R) Xeon(R) 2.20GHz CPU.

**4.2.1. Nonlinear problem I.** We consider the following variational problem as our first nonlinear test problem [21],

$$(4.4) \quad \begin{cases} \min_u \mathcal{F}(u(x, y)) = \int_{\Omega} \frac{1}{2} |\nabla u(x, y)|^2 + \gamma (u(x, y)e^{u(x, y)} - e^{u(x, y)}) \\ \quad - f(x, y)u(x, y) dx dy \\ \text{such that } u = 0 \quad \text{on } \partial\Omega, \end{cases}$$

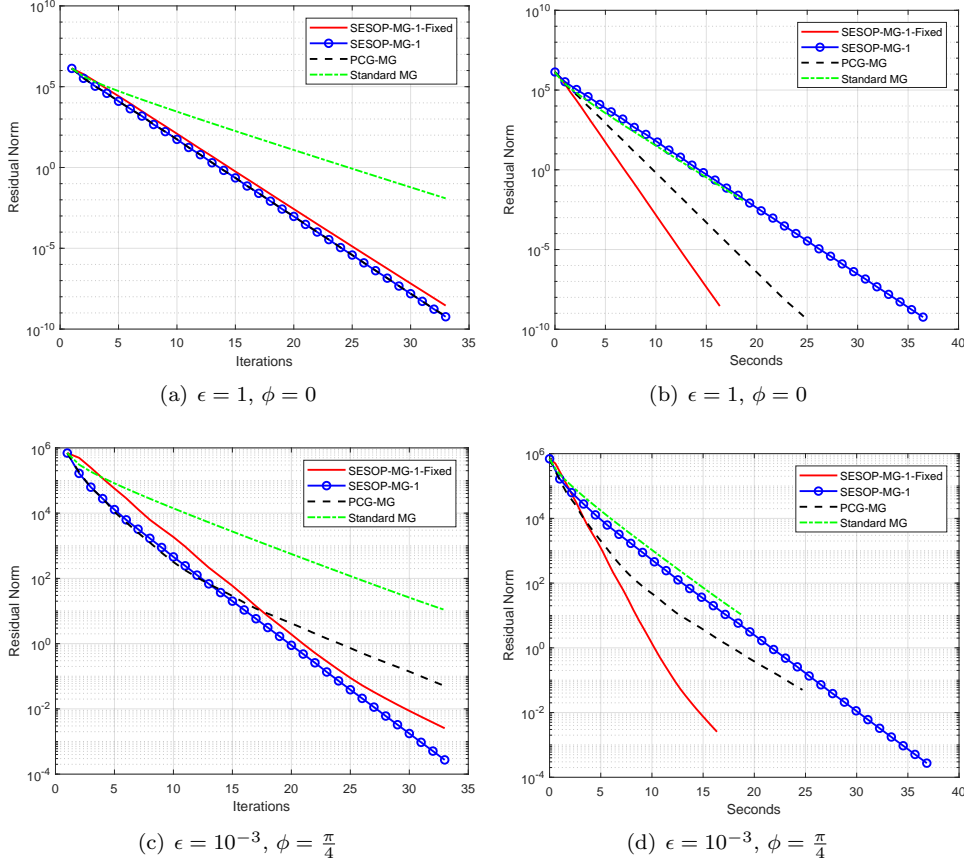


FIG. 4. Residual norm versus iterations and seconds with different  $\epsilon$  and  $\phi$  for the rotated anisotropic problem. We determine the stepsizes on  $64 \times 64$  grids and solve the problem on  $1024 \times 1024$  grids.

where  $\nabla$  is the differential operator,  $\gamma = 10$ ,  $\Omega = [0, 1] \times [0, 1]$ , and

$$f(x, y) = \left( (9\pi^2 + \gamma e^{(x^2 - x^3) \sin(3\pi y)}) (x^2 - x^3) + 6x - 2 \right) \sin(3\pi y).$$

Through the Euler-Lagrange equation, the gradient of (4.4) is

$$\nabla_u \mathcal{F} = h_x h_y (-\Delta u + \gamma u e^u - f),$$

where  $\Delta$  is the Laplacian operator,  $h_x$  and  $h_y$  denote the mesh-size on the  $x$  and  $y$  axes, respectively. Moreover, the analytic solution of (4.4) with the above  $f(x, y)$  is  $u(x, y) = (x^2 - x^3) \sin(3\pi y)$  [21, 5].

The number of grids on the finest level and the coarsest level is set to be  $1024 \times 1024$  and  $9 \times 9$ , respectively. Clearly, we have  $h_x = h_y = \frac{1}{1024}$ . Note that the equal mesh-size is assumed in the rest of this paper and denote by  $h$  for a uniform notation. The comparison of different methods for solving (4.4) is shown in Figure 5. Denote  $\mathcal{F}^*$  by the final objective value through substituting the analytic solution in (4.4). We clearly observe that SESOP-MG-1 yields the fastest convergence speed compared with other methods in terms of iterations and CPU time illustrating the significance of

involving the history. Moreover, we note that SD, Nesterov and LBFGS converge fast at the beginning of iterations but become slowly soon because they cannot eliminate the low frequency error efficiently demonstrating the potentiality of involving the CGC direction in our scheme.

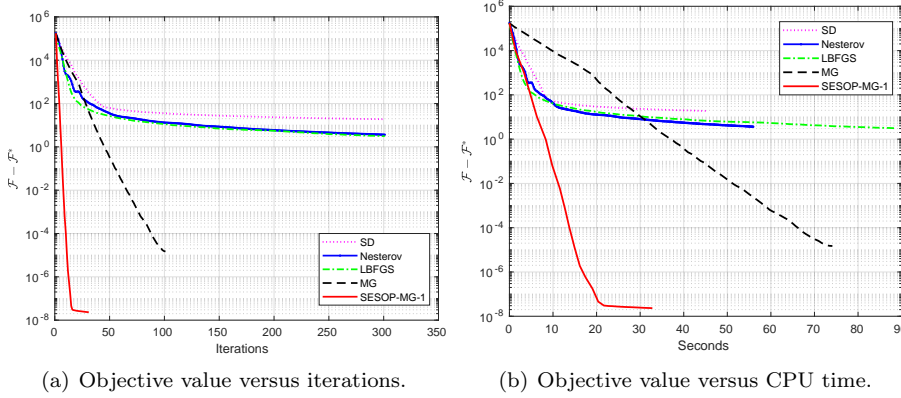


FIG. 5. The comparison of different methods for solving (4.4) on  $1024 \times 1024$  grids.

**4.2.2. Nonlinear problem II.** We take the following problem (called  $p$ -Laplacian) to investigate the performance of our approach further:

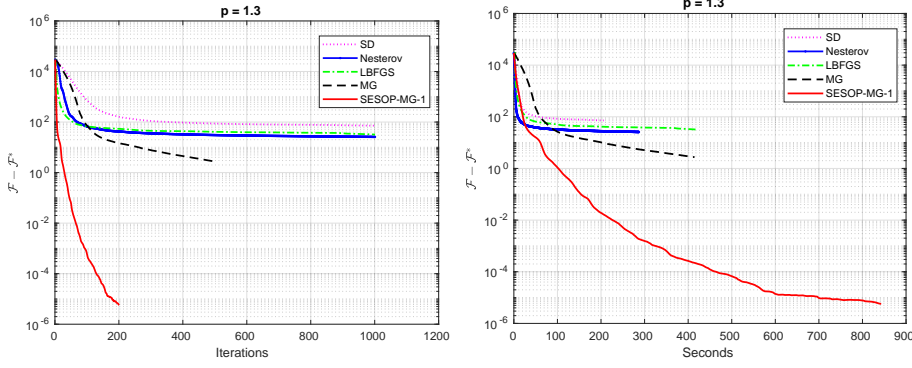
$$(4.5) \quad \begin{cases} \min_u \mathcal{F}(u(x, y)) = \int_{\Omega} \|\nabla u(x, y) + \xi\|^p - f(x, y)u(x, y) dx dy \\ \text{such that } u = 0 \text{ on } \partial\Omega, \end{cases}$$

where  $p \in (1, 2)$ . The corresponding PDE of (4.5) is:

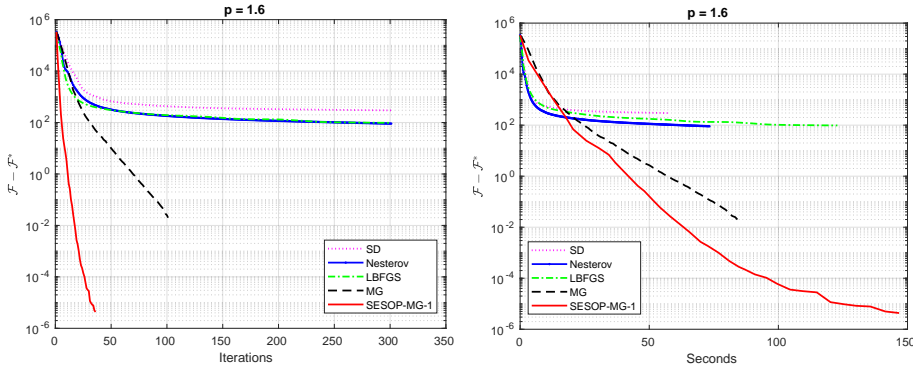
$$(4.6) \quad \begin{cases} -\nabla \cdot \left( \|\nabla u + \xi\|^{p-2} \nabla u \right) = f & \text{in } \Omega \\ u = 0 & \text{on } \partial\Omega. \end{cases}$$

The parameter  $\xi > 0$  is used as a regularization to avoid a trivial value in the denominator part. We set the true  $u(x, y)$  to be  $(x^2 - x^3) \sin(3\pi y)$  and obtain  $f(x, y)$  by substituting the true  $u(x, y)$  into (4.6). Denote by  $\mathcal{F}^*$  the final objective value obtaining by substituting the true  $u(x, y)$  and corresponding  $f(x, y)$  in (4.5). We note that solving (4.5) becomes challenge if  $p$  is close to 1 and relatively easy if  $p$  is close to 2. We choose two different  $p$  to test the performance of our approach, i.e.,  $p = 1.3$  and  $1.6$ . The corresponding results are shown in Figure 6. Clearly, we observe SESOP-MG-1 outperforms other methods in terms of iterations and CPU time in both cases. We note that other methods converge fast at the beginning of iterations but become slow soon which is the same as we observed from Figure 5 illustrating the benefit of adding the CGC direction in the subspace for eliminating the smooth error.

**Investing the influence of using different number of histories.** Now, we discuss the influence of choosing different size of histories for our approach. We apply the SESOP-MG with different size of histories to solving the  $p$ -Laplacian problem with  $p = 1.3$ . Observing from Figure 7(a), we find that adding necessary more histories yields a faster convergence speed. However, it becomes insignificant if we add too many histories. Moreover, using more histories means more CPU time is needed for the subspace minimization. As observed in Figure 7(b), we found using two histories



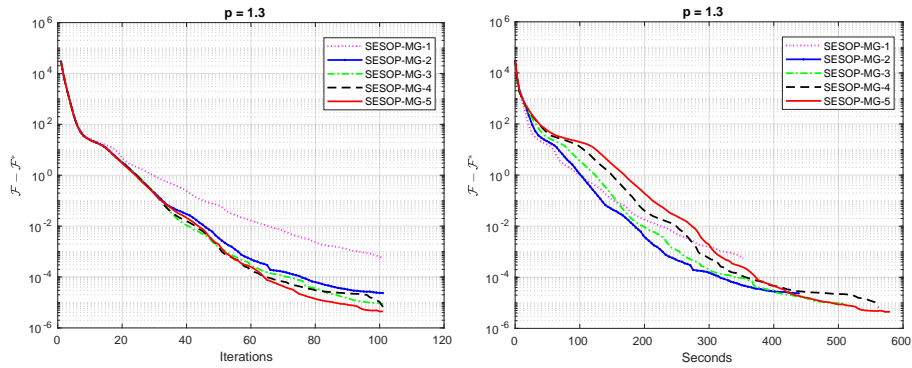
(a) Objective value versus iterations.  $p = 1.3$ . (b) Objective value versus CPU time.  $p = 1.3$ .



(c) Objective value versus iterations.  $p = 1.6$ . (d) Objective value versus CPU time.  $p = 1.6$ .

FIG. 6. The comparison of different methods for solving (4.5) on  $1024 \times 1024$  grids.

is a good trade-off to balance the convergence speed and the complexity of solving the subspace minimization problem in this test.



(a) Objective value versus iterations.  $p = 1.3$ . (b) Objective value versus CPU time.  $p = 1.3$ .

FIG. 7. Investigating the influence of using different number of histories for solving (4.5) with  $1024 \times 1024$  grids.

**5. Conclusions.** In this paper, we propose a novel scheme to accelerate the MG optimization. Our idea is to merge SESOP with MG methods by adding the CGC direction into the subspace  $\mathbf{P}_k$  yielding a faster algorithm than the standard MG methods. The smoothing analysis for linear problems and the numerical experiments illustrate the effectiveness and robustness of our novel scheme. Moreover, for elliptic PDEs with constant coefficients, we show that obtaining the optimal fixed stepsizes is relatively cheap if the local Fourier analysis is applied. Finally, we hope the novel scheme shown in this paper can be also used to solve the large-scale problems arising in signal processing and machine learning efficiently when the hierarchy can be defined well.

**Appendix A. The proof of Lemma 3.3.** Consider  $\hat{r}$  in (3.12) as a continuous function of a positive variable  $\lambda \in [\lambda_{min}, \lambda_{max}]$ , with fixed  $c_1$  and  $c_{23}$ :

$$\hat{r}(c_1, c_{23}, \lambda) = \frac{1}{2} \left| b(c_1, c_{23}, \lambda) + \operatorname{sgn}(b(c_1, c_{23}, \lambda)) \sqrt{b^2(c_1, c_{23}, \lambda) - 4c_1} \right|.$$

We distinguish between two regimes: (I):  $b^2 < 4c_1$  and (II):  $b^2 \geq 4c_1$ . In case (I), the square-root term is imaginary, and we simply get  $\hat{r} = \sqrt{c_1}$ . In case (II) the square-root term is real. Differentiating  $\hat{r}$  with respect to  $\lambda$  we then get

$$\frac{\partial \hat{r}}{\partial \lambda} = -\frac{c_{23}}{2} \operatorname{sgn}(b(c_1, c_{23}, \lambda)) \left[ 1 + \frac{|b(c_1, c_{23}, \lambda)|}{\sqrt{b^2(c_1, c_{23}, \lambda) - 4c_1}} \right]$$

We ignore the irrelevant choice  $c_{23} = 0$ , for which the method is obviously not convergent. Then, using  $b(c_1, c_{23}, \lambda) = c_{23} \left( \lambda - \frac{1+c_1}{c_{23}} \right)$ , we obtain

$$\frac{\partial \hat{r}}{\partial \lambda} = \frac{|c_{23}|}{2} \operatorname{sgn} \left( \lambda - \frac{1+c_1}{c_{23}} \right) \left[ 1 + \frac{|b(c_1, c_{23}, \lambda)|}{\sqrt{b^2(c_1, c_{23}, \lambda) - 4c_1}} \right].$$

We conclude that  $\hat{r}$  is evidently a symmetric function of  $\lambda - (1+c_1)/c_{23}$ , and it is furthermore convex, because its derivative is strictly negative for  $\lambda < (1+c_1)/c_{23}$  and positive for  $\lambda > (1+c_1)/c_{23}$ . It follows that, regardless of the sign of  $b^2 - 4c_1$  throughout the regime  $\lambda \in [\lambda_{min}, \lambda_{max}]$ , there exists no local maximum of  $\hat{r}$ . Hence,

$$(A.1) \quad \bar{r}(c_1, c_{23}) = \max(\hat{r}(c_1, c_{23}, \lambda_{min}), \hat{r}(c_1, c_{23}, \lambda_{max})).$$

This completes the proof.

**Appendix B. The proof of Lemma 3.4.**

Considering now  $\hat{r}(c_1, c_{23}, \lambda)$  as a continuous function of a real variable  $c_{23}$ , with  $c_1$  and  $\lambda$  fixed, we can apply the same arguments as in the previous lemma to show that  $\hat{r}$  is a convex symmetric function of  $c_{23} - \frac{(1+c_1)}{\lambda}$ . Differentiating  $\hat{r}$  with respect to  $c_{23}$ , we simply exchange the roles of  $\lambda$  and  $c_{23}$ , obtaining

$$\frac{\partial \hat{r}}{\partial c_{23}} = \frac{|\lambda|}{2} \operatorname{sgn} \left( c_{23} - \frac{1+c_1}{\lambda} \right) \left[ 1 + \frac{|b(c_1, c_{23}, \lambda)|}{\sqrt{b^2(c_1, c_{23}, \lambda) - 4c_1}} \right].$$

As in the previous lemma, it follows that the meeting point of  $\hat{r}(c_1, c_{23}, \lambda_{max})$  and  $\hat{r}(c_1, c_{23}, \lambda_{min})$ , which lies between  $c_{23} = (1+c_1)/\lambda_{max}$  and  $c_{23} = (1+c_1)/\lambda_{min}$ , is where  $\hat{r}$  is minimized with respect to  $c_{23}$ : for larger  $c_{23}$ ,  $\hat{r}(c_1, c_{23}, \lambda_{max})$  is at least as

large as at this point, while for smaller  $c_{23}$ ,  $\hat{r}(c_1, c_{23}, \lambda_{min})$  is at least as large. At the meeting point

$$1 + c_1 - c_{23}\lambda_{max} = -(1 + c_1 - c_{23}\lambda_{min}),$$

yielding

$$(B.1) \quad c_{23} = \frac{2(1 + c_1)}{\lambda_{min} + \lambda_{max}}.$$

This completes the proof.

**Appendix C. The proof of Lemma 3.5.** Note first that  $c_1^\pm$  are always real, because  $\mu \in (0, 1)$ , and positive, because

$$c_1^- = \frac{2}{\mu^2} - 1 - \frac{2}{\mu^2}\sqrt{1 - \mu^2} = \sqrt{\left(\frac{2}{\mu^2} - 1\right)^2} - \sqrt{\left(\frac{2}{\mu^2} - 1\right)^2 - 1} > 0.$$

We shall show that the derivative of  $\bar{r}$  is strictly negative for  $c_1 < c_1^-$ , whereas it is strictly positive for  $c_1 > c_1^-$ , so  $c_1^-$  is a unique minimizer. For  $c_1^- < c_1 < c_1^+$  the square-root term in (3.13) is imaginary. In this case we simply get  $\bar{r} = \sqrt{c_1^-}$ , whose derivative is clearly positive. (At the endpoints  $c_1^\pm$ , where the square-root term vanishes,  $\bar{r}$  is not differentiable.) For any  $c_1 \notin [c_1^-, c_1^+]$ , the expression  $\mu(1 + c_1) + \sqrt{\mu^2(1 + c_1)^2 - 4c_1}$  is positive so we can omit the absolute value operator in (3.13) in this regime, and the derivative with respect to  $c_1$  is then given by

$$(C.1) \quad \frac{\partial \bar{r}}{\partial c_1} = \frac{1}{2} \left( \mu + \frac{\mu^2(1 + c_1) - 2}{\sqrt{\mu^2(1 + c_1)^2 - 4c_1}} \right)$$

Note that  $\frac{\mu^2(1+c_1)-2}{\sqrt{\mu^2(1+c_1)^2-4c_1}}$  is positive for  $c_1 > \frac{2}{\mu^2} - 1$  and negative for  $c_1 < \frac{2}{\mu^2} - 1$ , hence, due to (3.14), it is positive for  $c_1^+$  and negative for  $c_1^-$ . Thus,  $\frac{\partial \bar{r}}{\partial c_1} > 0$  for  $c_1 > c_1^+$ , whereas for  $c_1 < c_1^-$  we have

$$\begin{aligned} \frac{\partial \bar{r}}{\partial c_1} &= \frac{1}{2} \left( \mu - \sqrt{\frac{(\mu^2(1+c_1)-2)^2}{\mu^2(1+c_1)^2-4c_1}} \right) = \frac{\mu}{2} \left( 1 - \sqrt{\frac{\mu^4(1+c_1)^2-4\mu^2(1+c_1)+4}{\mu^4(1+c_1)^2-4\mu^2c_1}} \right) \\ &= \frac{\mu}{2} \left( 1 - \sqrt{1 + \frac{4(1-\mu^2)}{\mu^4(1+c_1)^2-4\mu^2c_1}} \right) < 0 \end{aligned}$$

The last inequality is due to the fact that that  $0 < \mu < 1$  and that  $\mu^2(1+c_1)^2-4c_1 > 0$  in this regime, hence

$$\sqrt{1 + \frac{4(1-\mu^2)}{\mu^4(1+c_1)^2-4\mu^2c_1}} > 1.$$

We thus conclude that  $\frac{\partial \bar{r}}{\partial c_1} < 0$  for  $c_1 < c_1^-$  and  $\frac{\partial \bar{r}}{\partial c_1} > 0$  for  $c_1 > c_1^-$  (with a discontinuity in the derivative at  $c_1 = c_1^+$ ), implying that the minimum is attained at  $c_1 = c_1^-$ . This completes the proof.

#### REFERENCES

- [1] A. BORZÌ AND V. SCHULZ, *Multigrid methods for pde optimization*, SIAM review, 51 (2009), pp. 361–395.
- [2] A. BRANDT, *Multi-level adaptive solutions to boundary-value problems*, Mathematics of computation, 31 (1977), pp. 333–390.

- [3] A. BRANDT, *1984 multigrid guide with applications to fluid dynamics*, A. Brandt. Rigorous Local Mode Analysis of Multigrid, in Pref. Proc. SHALLOW-WATER BALANCE EQUATIONS, 25 (1985).
- [4] A. BRANDT AND O. E. LIVNE, *Multigrid techniques: 1984 guide with applications to fluid dynamics*, vol. 67, SIAM, 2011.
- [5] W. L. BRIGGS, S. F. MCCORMICK, ET AL., *A multigrid tutorial*, vol. 72, Siam, 2000.
- [6] M. ELAD, B. MATALON, AND M. ZIBULEVSKY, *Coordinate and subspace optimization methods for linear least squares with non-quadratic regularization*, Applied and Computational Harmonic Analysis, 23 (2007), pp. 346–367.
- [7] R. D. FALGOUT, P. S. VASSILEVSKI, AND L. T. ZIKATANOV, *On two-grid convergence estimates*, Numerical linear algebra with applications, 12 (2005), pp. 471–494.
- [8] S. GRATTON, M. MOUFFE, A. SARTENAER, P. L. TOINT, AND D. TOMANOS, *Numerical experience with a recursive trust-region method for multilevel nonlinear bound-constrained optimization*, Optimization Methods & Software, 25 (2010), pp. 359–386.
- [9] S. GRATTON, M. MOUFFE, P. L. TOINT, AND M. WEBER-MENDONÇA, *A recursive  $\ell_\infty$ -trust-region method for bound-constrained nonlinear optimization*, IMA Journal of Numerical Analysis, 28 (2008), pp. 827–861.
- [10] S. GRATTON, A. SARTENAER, AND P. L. TOINT, *Recursive trust-region methods for multiscale nonlinear optimization*, SIAM Journal on Optimization, 19 (2008), pp. 414–444.
- [11] P. HEMKER, *On the order of prolongations and restrictions in multigrid procedures*, Journal of Computational and Applied Mathematics, 32 (1990), pp. 423–429.
- [12] R. M. LEWIS AND S. G. NASH, *Model problems for the multigrid optimization of systems governed by differential equations*, SIAM Journal on Scientific Computing, 26 (2005), pp. 1811–1837.
- [13] G. NARKISS AND M. ZIBULEVSKY, *Sequential subspace optimization method for large-scale unconstrained problems*, Technion-IIT, Department of Electrical Engineering, 2005.
- [14] S. G. NASH, *A multigrid approach to discretized optimization problems*, Optimization Methods and Software, 14 (2000), pp. 99–116.
- [15] Y. NESTEROV, *Introductory lectures on convex optimization: A basic course*, vol. 87, Springer Science & Business Media, 2013.
- [16] C. W. OOSTERLEE AND T. WASHIO, *Krylov subspace acceleration of nonlinear multigrid with application to recirculating flows*, SIAM Journal on Scientific Computing, 21 (2000), pp. 1670–1690.
- [17] M. SCHMIDT, *minfunc: unconstrained differentiable multivariate optimization in matlab*, Software available at <http://www.cs.ubc.ca/~schmidtm/Software/minFunc.htm>, (2005).
- [18] K. STÜBEN, *An introduction to algebraic multigrid*, Multigrid, (2001), pp. 413–532.
- [19] P. L. TOINT, D. TOMANOS, AND M. WEBER-MENDONÇA, *A multilevel algorithm for solving the trust-region subproblem*, Optimization Methods & Software, 24 (2009), pp. 299–311.
- [20] U. TROTTEBERG, C. W. OOSTERLEE, AND A. SCHULLER, *Multigrid*, Academic press, 2000.
- [21] Z. WEN AND D. GOLDFARB, *A line search multigrid method for large-scale nonlinear optimization*, SIAM Journal on Optimization, 20 (2009), pp. 1478–1503.
- [22] R. WIENANDS AND W. JOPPICH, *Practical Fourier analysis for multigrid methods*, Chapman and Hall/CRC, 2004.
- [23] R. WIENANDS AND C. W. OOSTERLEE, *On three-grid fourier analysis for multigrid*, SIAM Journal on Scientific Computing, 23 (2001), pp. 651–671.
- [24] S. WRIGHT AND J. NOCEDAL, *Numerical optimization*, Springer Science, 35 (1999), p. 7.
- [25] J. XU AND L. ZIKATANOV, *Algebraic multigrid methods*, Acta Numerica, 26 (2017), pp. 591–721.
- [26] M. ZIBULEVSKY, *Speeding-up convergence via sequential subspace optimization: Current state and future directions*, arXiv preprint arXiv:1401.0159, (2013).
- [27] M. ZIBULEVSKY AND M. ELAD, *L1-l2 optimization in signal and image processing*, IEEE Signal Processing Magazine, 27 (2010), pp. 76–88.